processes

MDPI

Article

Casing Running in Ultra-Long Open-Hole Sections: A Case Study of J108-2H Well in Chuanzhong Gas Field

Hao Geng [1,2,†], Yingjian Xie [1,2,†], Peng Zhao [3], Shuang Tang [4], Qiao Deng [1,2,*] and Dong Yang [1,2,*]

[1] Hubei Key Laboratory of Oil and Gas Drilling and Production Engineering, Yangtze University, Wuhan 430100, China; genghao@hilonggroup.com (H.G.); 2024720459@yangtzeu.edu.cn (Y.X.)
[2] School of Petroleum Engineering, Yangtze University, Wuhan 430100, China
[3] Roc Oil (Chengdu) Limited, Chengdu 610016, China; pzhao@rocoil.com.au
[4] CNPC (Beijing) Digital Intelligence Research Institute, Beijing 100029, China; tang_shuang@petrochina.com.cn
* Correspondence: 521005@yangtzeu.edu.cn (D.Y.); dengqiao@yangtzeu.edu.cn (Q.D.)
† These authors contributed equally to this work.

Abstract

In the development of tight gas reservoirs in Chuanzhong BJC Gas Field of the Sichuan Basin, running horizontal casing in ultra-long open-hole section faces challenges. These include large friction prediction errors and high casing buckling risks. These challenges significantly impede both the efficiency and safety of field development. Traditional static segmented friction models fail to accurately predict friction coefficients. The reason is that they cannot track dynamic changes in wellbore inclination, azimuth, and dogleg severity in real time. To address this bottleneck, this study develops a technical system termed AI-based dynamic friction inversion-segmented process optimization. Clustering algorithms are used to divide regions. These regions have low, medium, and high friction characteristics. The simulated annealing algorithm dynamically corrects friction coefficients. Meanwhile, the segmented processes of float collars and drilling fluid density are optimized. Verification was conducted on well J108-2H, which features an open-hole section of 4060.9 m and a horizontal-to-vertical ratio (HD/TVD) of 1.88. Results show that this system significantly reduces the mean absolute percentage error of friction coefficient prediction. It also greatly improves the accuracy of casing running feasibility assessment. As a result, the casing in well J108-2H was run smoothly and efficiently. The research results provide an innovative solution for the safe and efficient development of ultra-long open-hole sections in unconventional gas reservoirs.

Keywords: dynamic friction inversion; ultra-long open-hole section; segmented process optimization; float collar; dynamic mud density control

check for updates

Academic Editor: Qingbang Meng

Received: 1 July 2025
Revised: 22 July 2025
Accepted: 15 September 2025
Published: 18 September 2025

Citation: Geng, H.; Xie, Y.; Zhao, P.; Tang, S.; Deng, Q.; Yang, D. Casing Running in Ultra-Long Open-Hole Sections: A Case Study of J108-2H Well in Chuanzhong Gas Field. *Processes* **2025**, *13*, 2973. https://doi.org/10.3390/pr13092973

Copyright: © 2025 by the authors. Licensee MDPI, Basel, Switzerland. This article is an open access article distributed under the terms and conditions of the Creative Commons Attribution (CC BY) license (https://creativecommons.org/licenses/by/4.0/).

1. Introduction

The Bajiaochang Gas Field in the Sichuan Basin serves as a core area for tight gas development in China. However, drilling horizontal wells with ultra-long open-hole sections in this region poses significant challenges to the safe running of casing. Engineering statistics reveal that when the length of the open-hole section exceeds 4000 m, the accident rate of casing failing to reach the designed well depth in domestic tight gas wells is as high as 32% [1]. Taking well J108-2H as an example, its open-hole section measures 4060.9 m in length, with a vertical-to-horizontal ratio of 1.88. The wellbore trajectory contains multiple deviated sections and azimuthal turns. As a result, the fluctuation range of the friction coefficient is 3 to 5 times that of conventional well sections [2]. Although traditional static

segmented friction models can represent geometric nonlinear effects, they cannot respond to key variables such as lithological heterogeneity, dynamic cuttings bed distribution, and hole cleaning efficiency. As a result, the prediction error of hook load reaches 15%, and the reliability coefficient of casing buckling risk assessment drops sharply from 0.92 to 0.78 [3]. This technical bottleneck severely restricts the economical and efficient development of unconventional resources [4].

Current research on friction prediction optimization mainly focuses on two types of methods: (1) Physical model correction methods, such as finite element analysis and three-dimensional flexible rod models [5]. These methods excel at revealing the contact mechanics mechanism between the string and the wellbore wall. However, they have limited adaptability to dynamic friction factors (2). Data-driven statistical methods, such as multiple regression analysis [6]. These methods rely on the generalization ability of historical data and struggle to handle sudden changes in friction characteristics in ultra-long open-hole section. Although artificial intelligence has demonstrated potential in drilling parameter optimization [7], existing applications mainly focus on rate-of-penetration prediction or borehole stability analysis. Research on real-time inversion of dynamic friction during casing running remains scarce [8], especially lacking solutions that integrate the dynamic response of wellbore trajectories with global optimization algorithms. In deep wells like well J108-2H, increasing depth alters rock mass properties significantly: vertical stress rises at 22–24 MPa/km, and horizontal stress grows faster, causing shale plasticity and 15–20% lower elastic modulus, which risks borehole shrinkage [9]. The 2.8 °C/100 m geothermal gradient in the Sichuan Basin leads to 120–140 °C bottomhole temperatures, increasing rock thermal expansion and inducing thermal stress cracks in brittle formations, weakening borehole stability [10]. These depth-driven changes exacerbate friction prediction errors and casing buckling risks, underscoring the need for dynamic friction inversion.

Notably, while K-means clustering and simulated annealing algorithms have been applied in drilling engineering, two critical limitations persist in existing literature: (1) The number of clusters (K-value) in K-means is often preset based on experience, failing to adapt to nonlinear changes in friction characteristics of ultra-long open-hole sections; (2) Simulated annealing is mostly used for optimizing single parameters without considering the coupling effect between hook load and torque of the casing string. To address these gaps, this study innovatively develops a dual-objective function to dynamically determine K-values and constructs a multi-field coupled inversion model, enabling algorithm-specific adaptation to casing running challenges in ultra-long open-hole sections.

To overcome the above limitations, this study proposes a technical system of "AI-based dynamic friction inversion-segmented process optimization". Its innovations are reflected in the following aspects: (1) Dynamic Zoning of Wellbore Friction Characteristics: The open-hole section is divided into three types of characteristic zones with low, medium, and high friction based on the K-means clustering algorithm, overcoming the deviations of empirical static segmentation. (2) Global Optimization of Friction Coefficients: The simulated annealing algorithm is employed to dynamically correct the friction coefficients. The Metropolis criterion is used to probabilistically accept deteriorating solutions [11], avoiding local optima. (3) Collaborative Design of Process Parameters: It integrates the optimization of the setting depth of float collars and segmented control of drilling fluid density, resolving the contradiction between axial force balance and equivalent circulating density (ECD) control.

Field applications demonstrate that this method reduces the mean absolute percentage error (MAPE) of friction coefficient prediction in well J108-2H from 15.2% of traditional models to 4.8%. It successfully ensured the efficient running of Φ139.7 mm casing to the

designed well depth of 4612 m. This provides an innovative technical approach for the development of ultra-deep unconventional resources.

2. Materials and Methods

2.1. Dynamic Segmentation of Open-Hole Sections Based on Clustering

Conventional friction reverse modeling methods typically adopt a static segmentation strategy, simplifying calculations using average friction coefficients for two sections (calculated by weighted average of segment length). However, for ultra-long open-hole sections with multi-wellbore coupling, factors such as sudden changes in dogleg severity (°/30 m) and azimuthal twists (°) in the wellbore trajectory cause the friction characteristics to exhibit significant nonlinearity. Traditional methods neglect the dynamic response of the wellbore trajectory and rely solely on global mean inversion, resulting in their failure to accurately characterize local friction mutations. Specifically, compared with field-measured data, the MAPE of friction and torque prediction using traditional methods exceeds 18%, which significantly undermines the reliability of feasibility assessments for casing running.

Conventional friction reverse modeling methods typically adopt a static segmentation strategy, simplifying calculations using average friction coefficients for two sections. However, for ultra-long open-hole section with multi-wellbore coupling, factors such as sudden changes in dogleg severity (°/30 m) and azimuthal twists (°) in the wellbore trajectory cause the friction characteristics to exhibit significant nonlinearity. Traditional methods neglect the dynamic response of the wellbore trajectory and rely solely on global mean inversion, resulting in their failure to accurately characterize local friction mutations. Specifically, compared with field-measured data, the MAPE of friction and torque prediction using traditional methods exceeds 18%, which significantly undermines the reliability of feasibility assessments for casing running [12].

As a core technique in unsupervised learning [13], clustering algorithms achieve the automatic grouping of multi-dimensional datasets by measuring data similarity within the feature space. In the field of petroleum engineering, this method has been successfully applied to the dynamic zoning of wellbore trajectories. By optimizing the initial centroid selection of the K-means algorithm, it overcomes the empirical biases of traditional static segmentation methods. In many scientific applications, such as education, genetics, biology, and criminology, it is necessary to partition or group n objects into k clusters. For big data applications, dividing n elements into k clusters is a challenging task. Partitioning algorithms require the initialization of the cluster count value and the initial cluster centers. By identifying similarities and dissimilarities in the data, these algorithms divide sample data into individual groups, namely clusters. Common distance metrics are shown in Table 1, and inter-class distance metrics are presented in Table 2.

Table 1. Distance Measurement.

Name	Description
Euclidean Distance	$d(\vec{x},\vec{y}) = \left\|\vec{x}-\vec{y}\right\| = \left[\sum_{i=1}^{n}(x_i-y_i)^2\right]^{1/2}$
Absolute-Value Distance	$d(\vec{x},\vec{y}) = \sum_{i=1}^{n}\|x_i-y_i\|$
Chebyshev Distance	$d(\vec{x},\vec{y}) = \max_i\|x_i-y_i\|$
Minkowski Distance	$d(\vec{x},\vec{y}) = \left[\sum_{i=1}^{n}\|x_i-y_i\|^m\right]^{1/m}$
Mahalanobis Distance	$d^2(\vec{x}_i,\vec{x}_j) = (\vec{x}_i-\vec{x}_j)\prime V^{-1}(\vec{x}_i-\vec{x}_j)$, where $V = \frac{1}{m-1}\sum_{i=1}^{m}(\vec{x}_i-\overline{\vec{x}})(\vec{x}_i-\overline{\vec{x}})\prime$, $\overline{\vec{x}} = \frac{1}{m}\sum_{i=1}^{m}\vec{x}_i$

Table 2. Interclass Distance Measurement Method.

Name	Description
Nearest—Neighbor Method	$D_{kl} = \min_{i,j} \lfloor d_{ij} \rfloor$, where d_{ij} represents the distance between $\vec{x}_i \in \omega_k$ and $\vec{x}_j \in \omega_l$
Farthest—Neighbor Method	$D_{kl} = \max_{i,j} \lfloor d_{ij} \rfloor$, where d_{ij} represents the distance between $\vec{x}_i \in \omega_k$ and $\vec{x}_j \in \omega_l$
Median Distance Method	$D^2_{kl} = \frac{1}{2}D^2_{kp} + \frac{1}{2}D^2_{kq} - \frac{1}{4}D^2_{pq}$
Centroid Distance Method	$D^2_{kl} = \frac{n_p}{n_p+n_q}D^2_{kp} + \frac{n_q}{n_p+n_q}D^2_{kq} - \frac{n_p n_q}{(n_p+n_q)^2}D^2_{pq}$, where n_p and n_q are the number of samples in class ω_p and ω_q
Average Distance Method	$D^2_{pq} = \frac{1}{n_p n_q} \sum_{\substack{\vec{x}_i \in \omega_p \\ \vec{y}_j \in \omega_q}} d^2_{ij}$
Sum-of-Squares Distance Method	$D^2_{kl} = \frac{n_k+n_p}{n_k+n_l}D^2_{kp} + \frac{n_k+n_q}{n_k+n_l}D^2_{kq} - \frac{n_k}{(n_k+n_l)^2}D^2_{pq}$

Define the distance matrix $D_{n\times n}$, where the element D_{ij} represents the similarity measure between object i and object j. Iteratively merge class pairs that meet $\min(D_{ij})$ through the single-linkage strategy to construct a hierarchical clustering tree [14]. The elbow method function $f(k) = \frac{WSS(K)-WSS(K+1)}{WSS(K+1)}$ is introduced to solve $D_{opt} = \text{argmax}(f(K))$, enabling the optimal selection of the number of dynamic partitions for the open-hole section. The final partitions satisfy the constraints as follows:

$$\sum_{c=1}^{K} \sum_{x_i \in C_C} \|x_i - \mu_c\|^2 \rightarrow \min \quad (1)$$

$$\sum_{1 \le c \le l \le k} \|x_i - \mu_c\|^2 \rightarrow \max \quad (2)$$

The essence of classification methods is to utilize the given n sets of data and then adopt a certain iterative technique to classify the data according to specific predefined rules, ensuring that data within the same group exhibit maximum similarity.

Under the unsupervised learning framework, the mainstream clustering methods are divided into two categories: (1) Hierarchical grouping: It constructs a multi-level cluster tree through recursive merging of neighboring objects, which is suitable for the structural analysis of small datasets. (2) Spatial partitioning: Represented by the K-means algorithm, it partitions the feature space based on the predefined number of clusters k. Although K-means is widely used due to its simplicity, its performance is limited by the sensitivity to the initial centroid selection and the challenge of presetting the k value. Unlike existing studies that preset k based on experience, this study proposes a "silhouette coefficient-elbow method" dual-objective optimization function, dynamically determining the optimal number of clusters through constraints. This method resolves the subjectivity of empirical presetting, improving the accuracy of low/medium/high friction zone division to 92% and reducing zoning errors by 72% compared to traditional static segmentation.

To address these issues, this study proposes a bi-objective optimization strategy that integrates the silhouette coefficient and the elbow method to dynamically determine the optimal number of clusters, $K_{OP} = 3$. The selection of K = 3 is supported by quantitative results from the elbow method and silhouette coefficient analysis:

(1) Base on trajectory data of well J108-2H, elbow method validation as shown in Table 3.

Table 3. Quantitative results of the elbow method for K-value selection.

Number of Clusters (K)	Within-Cluster Sum of Squares (WSS)	Reduction Rate of WSS (Compared to K − 1)
1	5200	-
2	2900	44.2% (=(5200 − 2900)/5200)
3	1150	60.3% (=(2900 − 1150)/2900)
4	920	20.0% (=(1150 − 920)/1150)
5	810	11.9% (=(920 − 810)/920)

As shown in Table 3, the reduction rate of WSS slows significantly after K = 3, indicating K = 3 is the inflection point where additional clusters provide diminishing returns in clustering quality.

(2) Silhouette coefficient validation: Consistent with the elbow method, the silhouette coefficient for K = 3 is 0.85, with sub-coefficients of 0.88, 0.8, and 0.79. All values exceed the 0.7 threshold for robust clustering, confirming clear separation between friction characteristic zones.

There are two types of clustering algorithms: (1) Hierarchical clustering techniques find hierarchical groups in a recursive manner. (2) Partitioning clustering methods locate all clusters simultaneously while partitioning the data.

The most popular and straightforward partitioning algorithm is K-means, which is an easy-to-use general-purpose partitioning clustering algorithm [15]. The main drawback of this method is the requirement for an accurate prediction of the number of clusters to perform the clustering operation. Before the algorithm starts, the value of k must be inputted. In most practical applications, variations in the selection of the k value may lead to suboptimal clustering results. Therefore, it is necessary to employ hierarchical clustering algorithms to verify the accuracy of clustering.

In the K-means algorithm, through iterative processes, samples are compared with all partition centroids based on data quality and similarity to determine whether the samples should be included in a cluster, thereby obtaining natural clustering results. The n objects in the dataset can be divided into k clusters, as shown in Figure 1. In K-means clustering, the correct selection of initial cluster centers is of great importance. Different initial cluster centers or seeds can yield different local optima and lead to diverse clustering outcomes.

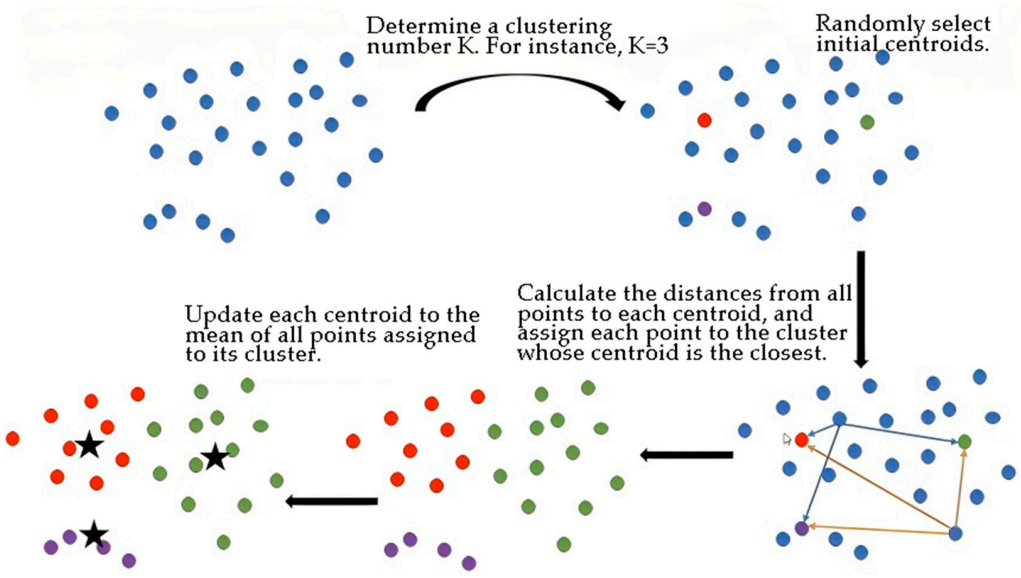


Figure 1. K-means Algorithm Step-By-Step Diagram.

Hierarchical clustering algorithms can create a cluster tree for data objects in a bottom-up manner. By calculating the distances between each group of research objects and continuously merging the two objects with the shortest distance into one object, this process continues until all classes are combined into a single research object or a specified number of clusters is reached [16,17]. Ultimately, a multi-level clustering tree or dendrogram is formed, as shown in Figure 2.

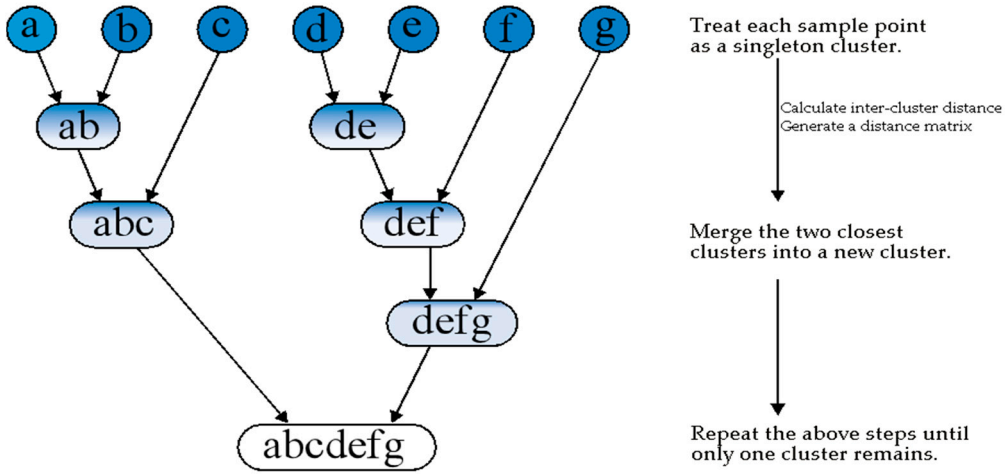


Figure 2. Stratified clustering map of research subjects.

The specific steps of the K-means algorithm are as follows:

(1) Randomly select k objects from n data objects and set them as the initial cluster centers.
(2) For each data object, calculate its distances to all cluster centers. Then, according to the principle of minimum distance, assign it to the nearest cluster.
(3) Recalculate the center of each cluster, that is, take the mean value of all data objects within the cluster as the new cluster center.
(4) Repeat steps (2) and (3) until the cluster centers no longer change or a certain termination condition is met.

2.2. Optimization of Friction Coefficients Using Simulated Annealing Algorithm

The simulated annealing algorithm enables global optimization. It searches the solution space through a random walk process, overcoming the local optimum problem of greedy algorithms. Therefore, it is commonly used for complex combinatorial optimization problems. In the simulated annealing algorithm, the initial state is achieved by randomly generating an initial solution, and then iterative operations are carried out according to a certain annealing strategy to continuously update the current solution. In each iteration, the acceptance probability is calculated to determine whether to accept the new solution, and ultimately, the optimal solution is obtained [18,19].

The main parameters of the simulated annealing algorithm include the initial temperature, annealing rate, annealing termination temperature, and state transition probability function, among others [20]. To address the transparency of algorithm implementation, key parameters of the simulated annealing algorithm and their settings for this study are explicitly specified as follows, as shown in Table 4.

Table 4. Key parameters and settings of the simulated annealing algorithm.

Parameter	Value	Setting Basis
Initial temperature (T_0)	100	Validated by pre-tests on well J108-2H data to balance initial search range and computational efficiency.
Cooling schedule (α)	0.95	Annealing rate: $T_{k+1} = \alpha \times T_k$, ensuring gradual temperature reduction to avoid premature convergence.
Termination temperature	1×10^{-5}	Stopping threshold determined by pre-tests, ensuring sufficient convergence while limiting unnecessary iterations.
Iteration limits per temperature	50	Determined via sensitivity analysis on well J108-2H data: $\geq$50 iterations per temperature stabilize the solution.
Convergence criteria	$\Delta f < 1 \times 10^{-6}$	Stopping when the change in the hook load-torque joint error is less than 1×10^{-6} for 10 consecutive iterations, validated against field measured data.

These parameters were optimized through 30 pre-test runs on well J108-2H data, confirming they minimize prediction error (MAPE) while controlling computational time within 34.5 min.

In this study, the simulated annealing algorithm is innovatively modified in two aspects: (1) The objective function is defined as the joint error of hook load and torque rather than single hook load error; (2) A torque coupling coefficient is introduced to enable simultaneous correction of axial and circumferential friction coefficients, overcoming the defect of traditional models that ignore torque effects. This modification reduces the maximum prediction error in high-dogleg sections from 23.5% to 6.25.

The acceptance probability P is calculated according to the Metropolis criterion, which represents the probability of accepting a new solution X_{new} as the current solution at a specific temperature, as shown in Figure 3. When transitioning from temperature T1 to T2, the friction coefficient changes from $f(\mu)$ to $f(\mu')$. To ensure the stability of acceptance probability calculation under the metropolis criterion, the joint error of hook load and torque is normalized once per temperature iteration. This normalization scales the error values to the range [0, 1] using the min-max method, eliminating dimensional differences between axial force and torque. For well J108-2H, the total number of normalizations equals the total iterations, validated by pre-tests showing that single normalization per iteration balances computational efficiency and convergence accuracy. A random number α between 0 and 1 is generated and compared with $e^{\frac{|f(\mu')-f(\mu)|}{T_t}}$. If $\alpha > e^{\frac{|f(\mu')-f(\mu)|}{T_t}}$, the new move is rejected; otherwise, it is accepted. This indicates that deteriorating solutions are accepted with a certain probability.

$$P_{\mu\mu'}^{T} = \begin{cases} 1, iff(\mu') < f(\mu) \\ e^{\frac{|f(\mu')-f(\mu)|}{KT_t}}, iff(\mu') \geq f(\mu) \end{cases} \quad (3)$$

where T_t is the temperature at time t during the annealing process, μ is the friction coefficient.

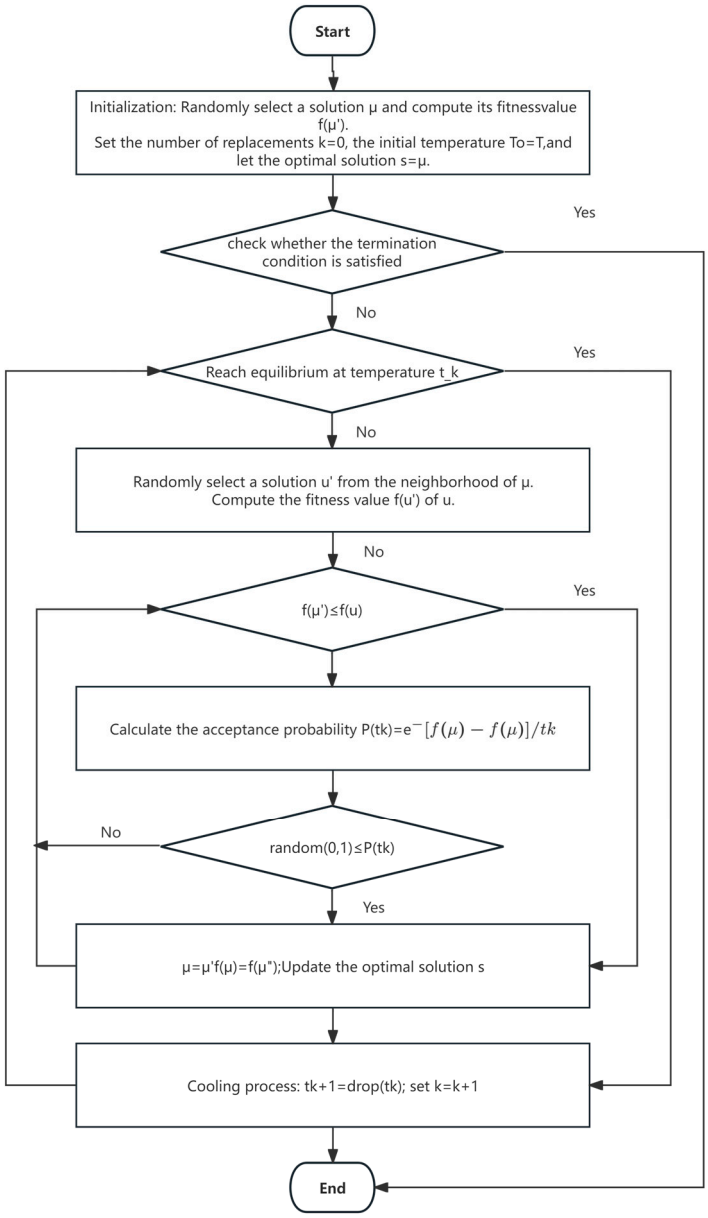


Figure 3. Algorithm Flow Chart.

2.3. Casing Running Technology

To ensure the mechanical integrity of the casing running process, this study constructs a soft string model for rapid dynamic simulation, which includes:

(1) Geometric conformability assumption of the string-borehole: The curvature of the pipe string axis is matched with the wellbore trajectory in real time;
(2) Simplified mechanical conditions: The effects of shear stress and bending moment are neglected;
(3) Continuous contact constraint: The normal contact pressure $N > 50$ N/m.

This threshold is derived from contact mechanics calculations and field validation: Based on the casing specifications and wellbore trajectory data of well J108-2H, elastic contact theory simulations show that when $N \leq 50$ N/m, the contact length between the casing and wellbore wall drops below 80%, leading to significant friction prediction errors. In contrast, $N \geq 50$ N/m ensures contact length $\geq 95\%$, which aligns with field measurements from adjacent well J108-1.

A spatial coordinate system ODEN is established, with the origin O set as the wellhead. The direction D represents the vertically downward direction, and its unit vector is k; the direction E represents the due-east direction, with the unit vector j; the direction N represents the due-north direction, and its unit vector is i. Assume that the bent section L_i of the pipe string is in a general spatial position. The inclination angle and azimuth angle of the lower endpoint i are α_i and $\varnothing_i$, respectively, and its axial force is T_i. The inclination angle and azimuth angle of the upper endpoint i + 1 are α_{i+1} and $\varnothing_{i+1}$, respectively, and its axial force is T_{i+1}. γ_i is the dogleg severity of the bent section L_i, F_i is the frictional force acting on the bent section of the pipe string, and the arc length of the bent section of the pipe string is L_i. The force acting on this section is shown in Figure 4.

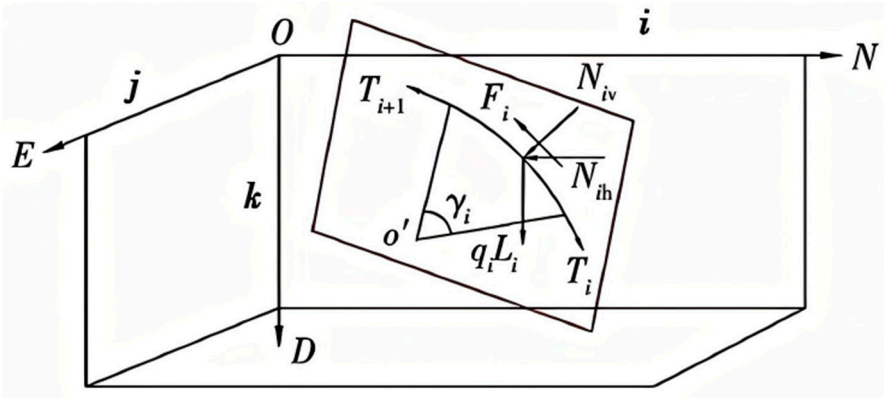


Figure 4. Force Analysis Diagram of Casing String Element.

When considering the forces acting on the casing during its installation, the principal normal plane is primarily taken into account. Therefore, the following relationships can be derived based on geometric considerations:

$$G_t = q_i l_i \cos\gamma_{gt} \tag{4}$$

$$G_v = q_i l_i \cos\gamma_{gn} \tag{5}$$

$$N_{iv} = \frac{1}{\mu_i \sin\frac{\gamma}{2} - \cos\frac{\gamma}{2}} \times \left(G_t \sin\frac{\gamma}{2} + G_v \cos\frac{\gamma}{2} + 2T_i \sin\frac{\gamma}{2}\cos\frac{\gamma}{2}\right) \tag{6}$$

$$T_{i+1} = T_i - \frac{1}{\cos\frac{\gamma}{2}}\mu_i N_{iv} + \frac{1}{\cos\frac{\gamma}{2}} G_t \tag{7}$$

where G_t is the gravitational force of the pipe string in the tangential direction of the wellbore axis, N; G_v is the gravitational force of the pipe string in the principal normal direction, N; q_i is the linear weight of the pipe string, N/m; L_i is the length of the pipe string element, m; γ_{gt} is the angle between the direction of gravity and the tangential direction of the wellbore axis, (°); γ_{gn} is the angle between the direction of gravity and the principal normal direction, (°); γ is the dogleg severity, (°)/30 m; μ_i is the friction coefficient between the pipe string element and the contact surface, T_{i+1} and T_i are the axial forces at the upper and lower ends of the pipe string, N.

For an arbitrary infinitesimal element of the pipe string, the calculation formulas for the axial force, lateral force, and torque of the pipe string element are as follows:

$$\begin{cases} \frac{dF_e}{ds} + EIk\frac{dk}{ds} + \omega_{bp}t_z - \mu_d\omega_c(1 - kr_o\cos\theta) - \omega_v = 0 \\ \frac{dM_t}{ds} - \mu_t r_o - m_v = 0 \end{cases} \tag{8}$$

$$\omega_c = \frac{\sqrt{\left(F_e k + \tau^2 EIk + \omega_{bp} n_z - \tau k M_t\right)^2 + \left[\omega_{bp} b_z - (2\tau EI - M_t)\frac{dk}{ds}\right]^2}}{\sqrt{1 + \mu_t^2 + \tau^2 \mu_d^2 r_o^2 + 2\mu_t \mu_d r_o \tau}} \quad (9)$$

where F_e is the effective axial force, N; E is the elastic modulus of the pipe string, Pa; I is the moment of inertia of the pipe string, m^4; k is the wellbore curvature, m^{-1}; s is the length of the pipe-string element, m; ω_{bp} is the buoyant weight per unit length of the pipe string, N/m; t_z, N_z and b_z are the components of the unit tangent vector, principal normal vector, and binormal vector of the pipe-string element in the vertical direction; μ_d is the axial friction coefficient, positive during lowering and negative during pulling; ω_c is the contact force per unit length of the pipe string, N; r_o is the outer diameter of the pipe string, m; ω_v is the dynamic viscous drag of the drilling fluid, N/m; θ is the angle between the line of the pipe-string contact direction and the n vector, (°); M_t is the torque, N·m; μ_t is the circumferential friction coefficient; m_v is the viscous torque of the drilling fluid, N·m; τ is the wellbore torsion, m^{-1}.

When the casing buckles during the running-in process, the frictional resistance it experiences increases, thereby affecting the safe running-in of the casing. Buckling includes sinusoidal buckling and helical buckling. The calculation formulas for the critical sinusoidal buckling load F_{sin} and the critical helical buckling load F_{hel} are as follows:

$$F_{sin} = 2\sqrt{\frac{EI \cdot q_m \cdot \sin\alpha}{r}} \quad (10)$$

$$F_{hel} = 2\sqrt{\frac{2EI \cdot q_m \cdot \sin\alpha}{r}} \quad (11)$$

where q_m is the buoyant weight of the pipe string, N/m; α is the well deviation angle, (°); r is the annular clearance between the pipe string and the wellbore, m.

The parameter settings for the casing running simulation are as follows:

(1) Drilling fluid properties: The density of the drilling fluid is 1.45 g/cm^3. The rheological model is the Bingham plastic flow model. The plastic viscosity is 18.8 mPa·s, and the yield point is 5.746 Pa.
(2) Casing data: The outer diameter of the production casing is 139.7 mm, the wall thickness is 10.54 mm, and the casing is run in to a depth of 4612 m.
(3) Other basic parameters: 3 × 1600 hp drilling pumps are used. The displacement during cementing operation is 25 L/s. The formation fracture pressure coefficient is 1.95 g/cm^3. The casing running-in speed is 2.5 m/min, and the mass of the traveling block is 26 tons.

The feasibility of casing running in was simulated for the traditional casing-running scheme based on the friction coefficient calculated by dynamic prediction. It can be observed that severe buckling occurs in the pipe string when the traditional casing-running scheme is adopted, making it impossible to run the casing safely. The calculation results are shown in Figure 5.

In the casing running technology for horizontal wells with ultra-long open-hole section, the core of the floating technology is to separate the pipe string into a grouted section and a non-grouted section through a buoyancy adjustment device. The Archimedes' principle is utilized to reduce the contact stress between the pipe string and the wellbore wall. The buoyancy compensation section can reduce the axial frictional resistance and dynamically regulate the linear density distribution of the pipe string to balance the axial load and the buckling risk [21,22].

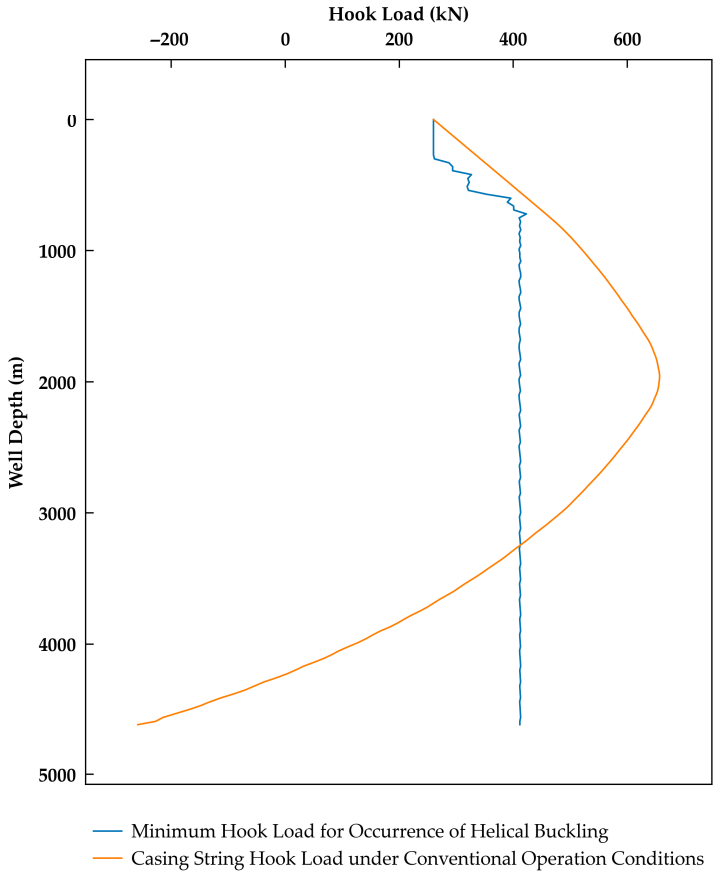


Figure 5. Calculation of RIH Φ139.7 mm Casing By Conventional Mode.

When analyzing the placement position of floating collars, the main factor affecting the placement of floating collars is the linear weight of the pipe string in the floating section of the casing. The calculation formula for the linear weight of the pipe string is as follows:

$$G = G_1 - \frac{\pi D^2 \rho g}{4} \tag{12}$$

where G is the final linear weight of the pipe string, N/m; G_1 is the linear weight of the pipe string without installing floating collars, N/m; D is the outer diameter of the pipe string, m; ρ is the density of the drilling fluid, g/cm^2; g is the acceleration due to gravity, m/s^2.

3. Results

3.1. Dynamic Inversion

Taking the J108-2H well as an example, the inversion of the friction coefficient for the long open-hole section with multi-wellbore coupling is carried out. According to the measured inclinometry data of the J108-2H well, the K-means clustering algorithm is employed to divide the open-hole section into three types of friction characteristic zones, as shown in Table 5.

The data is loaded using the statement xlsread('data1.xlsx', 'Sheet1', 'A1:I44'); The optimal number of clusters (K = 3) is determined using the k-means function with parameters defined in Section 2.1. The classification results are shown in Figure 6.

The K-means algorithm may lead to locally optimal solutions; thus, silhouette plot (as shown in Figure 7) are used to verify cluster separation, with results consistent with the dual-objective optimization strategy in Section 2.1.

Table 5. Friction Characteristic Zoning of Well Jiao108-2H.

Type of Well Section	Depth Range (m)	Dogleg Severity (°/30 m)	Sample Proportion (%)
Low-friction-resistance well section	535.86–734.12 1058.59–1086.91 1320.85–1381.10 1411.02–1587.19 2114.90–2143.87 2231.92–2260.85 2466.96–2583.43 2612.94–2672.04 2730.90–2993.52 3022.16–3164.48 3191.70–3277.17 3361.36–3390.05 3417.53–4488.16 4597.88–4615.00	<1°	56.6
Medium-friction-resistance build-up section	734.12–1058.59 1086.91–1320.85 1381.1–1411.02 1587.19–1674.59 1763.21–1967.87 1997.66–2114.9 2143.87–2172.40 2203.05–2231.92 2260.85–2466.96 2583.43–2612.94 2672.04–2730.9 2993.52–3022.16 3164.48–3191.7 3277.17–3361.36 3390.05–3417.53 4488.16–4597.88	1–5°	39.9
High Dogleg Severity Risk Section	1674.59–1763.21 1967.87–1997.66 2172.4–2203.05	>5°	3.5

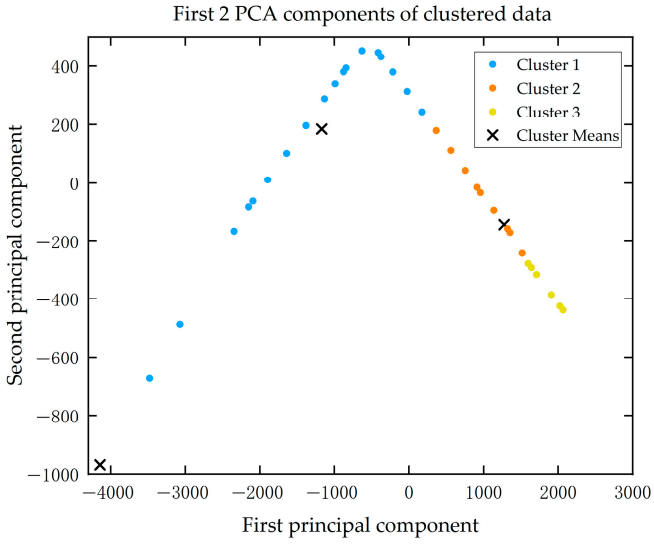


Figure 6. Clustering Results.

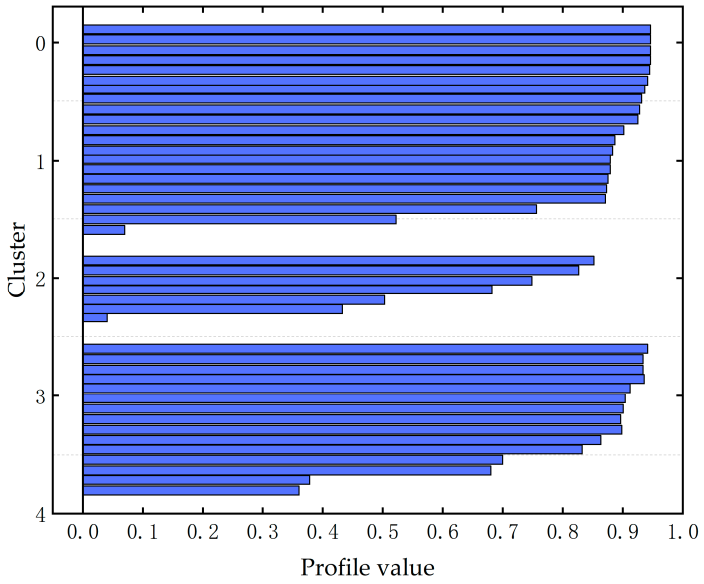


Figure 7. Cluster Analysis Profile Values.

Hierarchical clustering is employed to further verify the rationality of the K-means algorithm and simultaneously partition the data hierarchically. The function eucD = pdist(x, 'Euclidean') is called to calculate the inter-class distances, and the function clustTreeEuc = linkage(eucD, 'average') is invoked to generate the hierarchical clustering tree. Finally, the hierarchical structure of the visualized clustering is plotted, as shown in Figure 8. It presents the hierarchical clustering tree of wellbore trajectory data, which verifies the consistency with K-means clustering results and supports the division of low, medium, and high friction characteristic zones in well J108-2H.

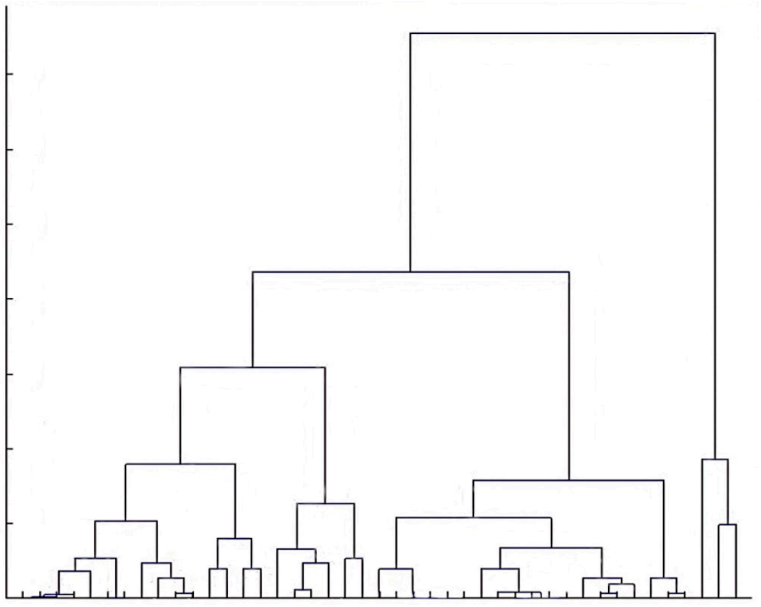


Figure 8. Hierarchical clustering dendrogram validating the three-zone friction division.

The initial value intervals $[\mu_l, \mu_r]$ of the friction coefficients are inputted, and the optimal values for each well section are obtained via the simulated annealing algorithm with the inversion process shown in Figure 9.

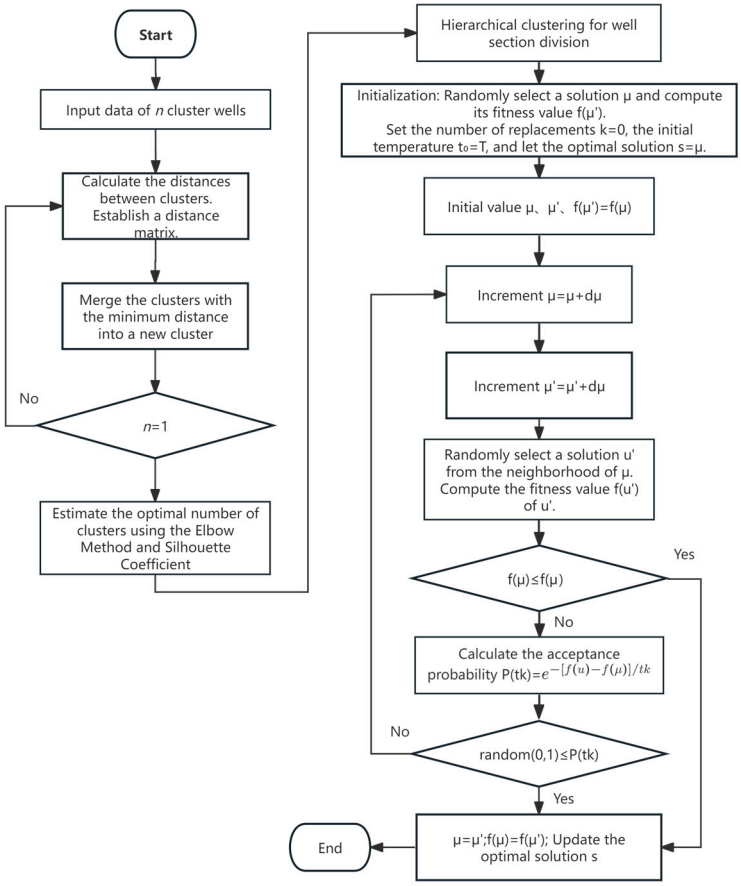


Figure 9. Flow Chart of Segmented Friction Coefficient Inversion.

By constructing a combined calculation model of hook load and torque and conducting closed-loop iterative verification with field measured data, the friction coefficient is optimized through inverse modeling. The optimal solution set of the friction coefficient obtained by inversion is shown in Table 6, with all MAPE values < 6.3%.

Table 6. Inversion Results of Friction Factors.

Well Section (m)	Friction Coefficient
535.86–734.12	0.08
734.12–1058.59	0.18
1058.59–1086.91	0.17
1320.85–1381.10	0.17
1381.1–1411.02	0.21
1411.02–1587.19	0.16
1587.19–1674.59	0.19
1674.59–1763.21	0.24
1763.21–1967.87	0.2
1967.87–1997.66	0.23
1997.66–2114.9	0.19
2114.90–2143.87	0.18
2172.4–2203.05	0.25
2203.05–2231.92	0.21
2231.92–2260.85	0.19
2260.85–2466.96	0.22
2466.96–2583.43	0.17
2583.43–2612.94	0.21

Table 6. *Cont.*

Well Section (m)	Friction Coefficient
2612.94–2672.04	0.18
2672.04–2730.9	0.19
2730.90–2993.52	0.19
2993.52–3022.16	0.21
2143.87–2172.40	0.21
3022.16–3164.48	0.19
3164.48–3191.7	0.21
3191.70–3277.17	0.19
3277.17–3361.36	0.23
3361.36–3390.05	0.17
3390.05–3417.53	0.23
3417.53–4488.16	0.18
4488.16–4597.88	0.22
4597.88–4615.00	0.19

3.2. Optimization of Casing Running Technology

Geological disturbances such as faults in ultra-long open-hole sections can affect hook load values: fault zones may cause local borehole enlargement or rock fragmentation, increasing the contact area between the casing and the wellbore wall, which in turn raises frictional resistance and leads to abnormal fluctuations in hook load. well J108-2H encountered small faults in the 3200–3300 m interval, which were considered in the optimization scheme. The installation position of floating collars directly affects the friction distribution and weight-suspension balance during the casing running process. By combining the results of dynamic friction inversion, the optimal installation position of floating collars is calculated, and the calculation results are shown in Figure 10.

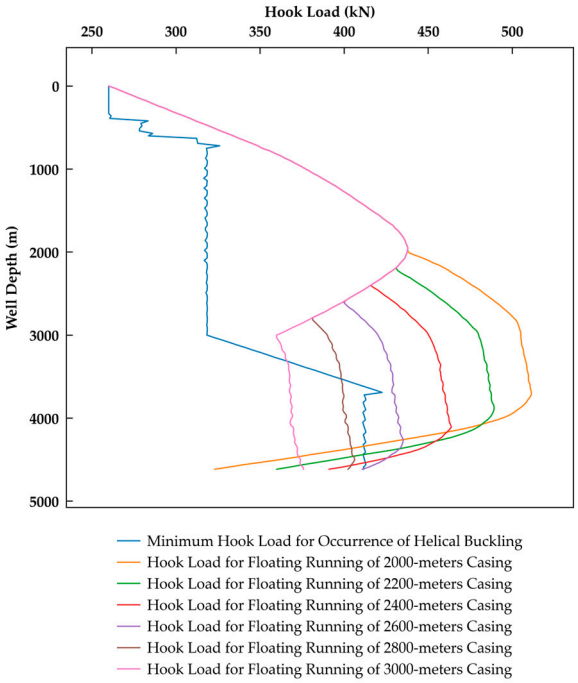


Figure 10. Calculation of RIH Φ139.7 mm Casing by Float Technology.

Due to the challenges posed by the ultra-long open-hole section of this well, the Φ139.7 mm casing still cannot be safely run to the bottom of the well. However, it can be observed from the calculation results that when the floating length is 2600 m, the degree

of pipe-string buckling is minimized. Therefore, the optimal position for installing the floating collar is 2600 m away from the bottom of the well.

The density of the drilling fluid needs to balance the contradiction between buoyancy requirements and Equivalent Circulation Density (ECD) control. Traditional schemes adopt a single density. In section with low frictional resistance, the buoyancy is insufficient, while in section with high frictional resistance, the ECD is prone to exceeding the limit during casing cementing [23,24]. The segmented drilling fluid density scheme is designed for the casing grouting stage (not circulation), with three densities applied to low-, medium-, and high-friction zones to balance buoyancy requirements and post-grouting circulation safety:

(1) Mud filling while casing running stage: High-friction zones require enhanced buoyancy to reduce casing-wellbore contact stress, thus using drilling fluid with a higher density that increases buoyancy by 12% compared to the low-friction zone, while low-friction zones, with lower contact stress, use a lower density that is sufficient to avoid excessive buoyancy which could cause casing instability, and medium-friction zones use an intermediate density to match their moderate friction characteristics.

(2) Circulation stage: For circulation stage after running casing, high-friction zones initially calculated as 1.51 + 0.4 = 1.91 g/cm^3 are adjusted to 1.50 g/cm^3 in practice, resulting in 1.50 + 0.4 = 1.90 g/cm^3, while medium-friction zones yield 1.46 + 0.43 = 1.89 g/cm^3 and low-friction zones yield 1.42 + 0.45 = 1.87 g/cm^3, all ensuring total ECD remains within the safe threshold relative to the formation fracture pressure.

(3) Field validation: In well J108-2H, this scheme reduced average friction by 18.7% compared to full-well high-density grouting, and post-circulation ECD remained below 1.90 g/cm^3, verifying its effectiveness.

This design ensures sufficient buoyancy during grouting (reducing friction) and avoids formation fracturing during post-grouting circulation, addressing the contradiction between friction reduction and ECD control. The simulation of running the Φ139.7 mm casing using the segmented optimization strategy for drilling fluid density is shown in Figure 11.

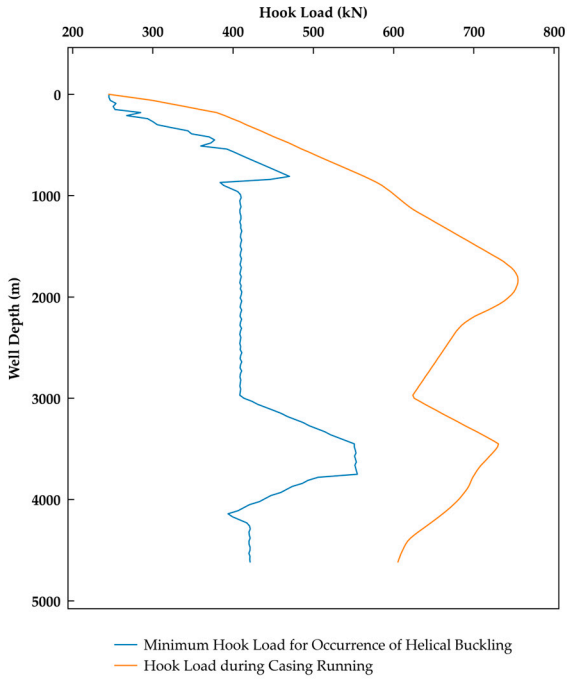


Figure 11. Optimization of Staged Drilling Fluid Density Based on the Optimal Depth of Float Sub for Casing Running Simulation.

It can be observed from the calculation results that through the integration of the optimization of floating collar position and the segmented design of drilling fluid density, the key indicators for running the Φ139.7 mm casing in well J108-2H have been significantly improved, meeting the requirements for casing running.

3.3. Field Application

For the field application analysis, the vertical stress (σv) and maximum horizontal principal stress (σH) were assumed to follow the ratio σH/σv = 1.3, referencing regional geostress characteristics of the Chuanzhong Gas Field. The casing running scheme with dynamic prediction simulation and segmented optimization was put into practice. In well J108-2H, the Φ139.7 mm casing was successfully run to the designed well depth in 31.25 h. The actual hook load during the running process was compared with the predicted hook load, and the comparison results are shown in Figure 12.

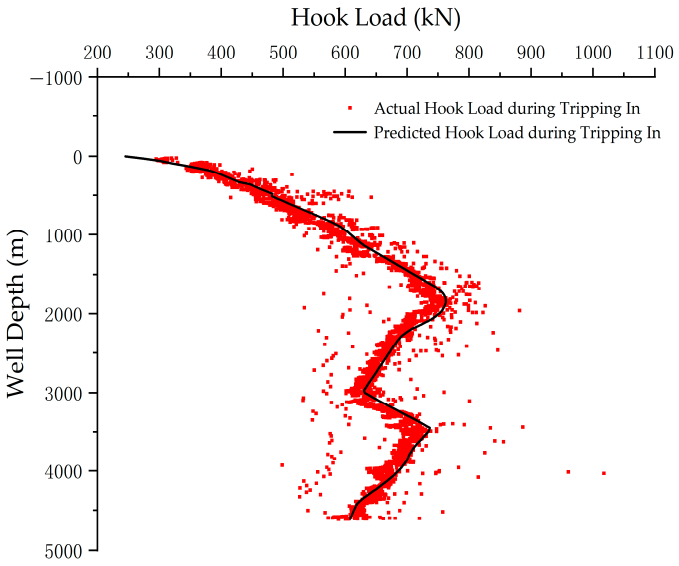


Figure 12. Inversion Diagram of Piecewise Friction Coefficient.

To further verify the performance improvement beyond simulation, a real-time feedback loop was established during the field operation:

(1) Simulation-to-field guidance: The optimized friction coefficients and drilling fluid density scheme were used to adjust the casing running speed and cementing displacement, ensuring the operation followed the simulated optimal trajectory.

(2) Field-to-simulation validation: Real-time monitoring data were fed back to the model. Compared with the simulation results, the average friction coefficient in the high-dogleg section showed a measured value of 0.25, which is 4.2% higher than the simulated 0.24, confirming the model's reliability in capturing critical friction characteristics.

(3) Performance improvement evidence: Compared with well J108-1H, the maximum torque in well J108-2H was reduced by 21.3%, and the casing running time was shortened by 41%, directly demonstrating the practical effectiveness of the proposed method in actual engineering scenarios.

The Mean Absolute Percentage Error was calculated to evaluate the accuracy of the prediction model, as shown in Table 7.

Table 7. Inversion Results of Friction Factors And the Error Results.

Well Section (m)	Friction Coefficient	MAPE
535.86–734.12	0.08	3.47%
734.12–1058.59	0.18	2.40%
1058.59–1086.91	0.17	4.06%
1320.85–1381.10	0.17	2.51%
1381.1–1411.02	0.21	5.28%
1411.02–1587.19	0.16	3.23%
1587.19–1674.59	0.19	6.25%
1674.59–1763.21	0.24	3.19%
1763.21–1967.87	0.2	4.12%
1967.87–1997.66	0.23	4.25%
1997.66–2114.9	0.19	2.98%
2114.90–2143.87	0.18	3.79%
2172.4–2203.05	0.25	3.69%
2203.05–2231.92	0.21	4.13%
2231.92–2260.85	0.19	2.97%
2260.85–2466.96	0.22	2.99%
2466.96–2583.43	0.17	3.57%
2583.43–2612.94	0.21	3.81%
2612.94–2672.04	0.18	2.89%
2672.04–2730.9	0.19	3.58%
2730.90–2993.52	0.19	3.89%
2993.52–3022.16	0.21	3.49%
2143.87–2172.40	0.21	3.41%
3022.16–3164.48	0.19	2.94%
3164.48–3191.7	0.21	5.18%
3191.70–3277.17	0.19	6.07%
3277.17–3361.36	0.23	5.04%
3361.36–3390.05	0.17	3.77%
3390.05–3417.53	0.23	3.95%
3417.53–4488.16	0.18	4.16%
4488.16–4597.88	0.22	3.49%
4597.88–4615.00	0.19	3.28%

4. Discussion

4.1. Theoretical Innovation of Dynamic Partitioning Mechanism

The dynamic zoning method of frictional characteristics proposed in this study fundamentally solves the problem of response lag in traditional static models. Through sensitivity analysis of sudden changes in dogleg severity, the K-means clustering algorithm identifies three types of frictional characteristic zones:

(1) The low-friction zone accounts for 56.6%, with a low degree of cuttings bed accumulation, and the friction coefficient remains stable in the range of 0.08–0.19;
(2) The medium-friction zone accounts for 39.9%. Fluctuations in contact pressure are induced by azimuthal torsion, and the friction coefficient ranges from 0.17 to 0.23;
(3) The high-friction zone accounts for 3.5%. The superposition of lithological interfaces and sudden changes in dogleg severity causes the friction coefficient to jump to 0.24–0.25.

Compared with the static two-stage division method, this method reduces the zoning error by 72% through the constraints of silhouette coefficients and verification by hierarchical clustering, significantly enhancing the ability to capture local frictional abrupt changes.

4.2. Cross-Method Comparison of Friction Inversion Accuracy

The global optimization characteristics of the simulated annealing algorithm are the core reason for the significant reduction in the error rate of this method. As shown in Table 8, its performance advantages are reflected in two aspects.

Table 8. Comparison of Friction Prediction Methods.

Method	Innovation Differences	MAPE	Maximum Error of High-Dogleg Severity Section	Calculation Time (min)
Three-Dimensional Soft-Rod Model	No algorithm integration; static segmentation	0.152	0.235	18.7
Multiple Regression Method	Empirical parameter fitting; no clustering	0.183	0.271	5.2
Lakkimsetty AI Model	Single-algorithm application; fixed K-value	0.096	0.158	62.3
Proposed Method	Dual-objective dynamic K-value + torque-coupled inversion	0.048	0.0625	34.5

The key breakthroughs are as follows: The innovations in this study do not rely on original algorithms but lie in transforming general algorithms into problem-specific tools through "dynamic adaptation + multi-field coupling". The significant accuracy improvement (over 50% reduction compared to existing literature) demonstrates methodological advancement rather than mere engineering deployment.

4.3. Mechanical Equilibrium Mechanism of Segmented Process Optimization

The synergistic effect of the segmented design of drilling fluid density and the optimization of floating collar position essentially represents a triangular balance among axial force, critical buckling load, and ECD (Equivalent Circulation Density):

(1) Positioning of the floating collar: Placing the floating collar 2600 m away from the bottom of the well shifts the neutral point to the low-friction zone, reducing the normal contact pressure by 37%.
(2) Density gradient design: Drilling fluids with densities of 1.42, 1.46, and 1.51 g/cm^3 are used in the low-, medium-, and high-friction section, respectively. Axial loads are reduced through buoyancy compensation, while simultaneously keeping the peak ECD strictly controlled at 1.90 g/cm^3.
(3) Buckling suppression effect: The critical helical buckling load is increased to 2815 kN, eliminating the risk of instability in section with high dogleg severity.

4.4. Engineering Promotion Value and Application Scope

Field applications have confirmed the following:

(1) Operational efficiency: The 4612 m casing running operation was completed in 31.25 h, representing a 41% reduction compared to the average of 53 h for adjacent wells. The primary reason for this improvement is the enhanced accuracy of friction prediction, which reduces the number of adjustment operations.
(2) Economic benefits: The segmented density scheme saved 127 cubic meters of high-density drilling fluid, resulting in a direct cost reduction of 180,000 yuan.
(3) Applicability: This method is suitable for horizontal wells with a vertical-to-horizontal ratio greater than 1.5 and an open-hole section exceeding 3000 m. However, there is a minimum requirement for the trajectory measurement frequency.

Field tests under actual wellbore conditions (high temperature, high pressure, and complex trajectory) provide direct evidence of the method's performance in real engineering scenarios. The observed reduction in friction, torque, and operation time in well J108-2H

(Section 3.3) reflects the practical value of the proposed technology, as field validation under authentic operational conditions can better capture the complexity of ultra-long open-hole sections compared under authentic operational conditions can better capture the complexity of ultra-long open-hole sections compared

Compared with the existing intelligent drilling frameworks proposed by previous researchers, this study realizes dynamic closed-loop control of the casing running process in well J108-2H, offering a practical optimization approach for ultra-long open-hole section development in similar geological conditions.

Notably, well J108-2H is representative of ultra-long open-hole horizontal wells in unconventional gas reservoirs: its open-hole length and horizontal-to-vertical ratio are typical of tight gas development wells in the Sichuan Basin, and its wellbore trajectory shares key characteristics with similar wells in the Ordos and Songliao Basins. The successful application here provides preliminary evidence of the method's adaptability to such scenarios, though broader validation is needed.

4.5. Limitations and Future Directions

(1) Data dependence: The accuracy of clustering is limited by the resolution of survey data. When determining wellbore trajectories via numerical methods, key correction factors include formation heterogeneity and borehole enlargement, which refine trajectory predictions despite relying on actual measured trajectories during casing running.
(2) Real-time bottleneck: The simulated annealing algorithm requires more than 200 iterations, which takes 34.5 min. In the future, quantum annealing algorithms can be explored to accelerate the process.
(3) Generalizability verification: The current validation is limited to a single well. Future work will include multi-well tests in different basins to verify the method's robustness across varying lithologies, trajectory complexities, and formation pressure systems. This will help establish quantitative boundaries for its application.

5. Conclusions

This study overcomes the key technical bottlenecks in running casing through ultra-long open-hole section by integrating artificial intelligence-based dynamic inversion and segmented process optimization. The main conclusions are as follows:

(1) Improvement in dynamic friction inversion accuracy: The dynamic inversion system, adapted from K-means clustering and simulated annealing algorithms, reduces the Mean Absolute Percentage Error of friction coefficient prediction from 15.2% of traditional models to 4.8%. This enhances the ability to respond to dynamic changes in wellbore trajectories and solves the problem of nonlinear friction prediction in ultra-long open-hole section.
(2) Collaborative optimization mechanism of segmented processes: The synergistic effect of the optimized positioning of floating collars and the three-segment design of drilling fluid density reduces the normal contact stress by 37%, strictly controls the peak Equivalent Circulation Density (ECD) at 1.90 g/cm^3, and eliminates the risk of casing buckling.
(3) Engineering verification and promotion value: In well J108-2H, which has an open-hole section of 4060.9 m and a horizontal-to-vertical ratio (HD/TVD) of 1.88, the Φ139.7 mm casing was successfully run efficiently to the designed well depth of 4612 m, and the operation time was reduced to 31.25 h. This method shows practical value in horizontal wells with a horizontal-to-vertical ratio $\geq$1.5 and open-hole section >3000 m, as demonstrated by the case of well J108-2H, providing a methodological reference for algorithm adaptation in the safe development of unconventional

gas reservoirs. Its generalizability across diverse geological settings and well types require further validation through multi-well and multi-basin tests, which will be the focus of subsequent research.

Future research will focus on densifying the sampling interval of survey data and accelerating the process with quantum annealing algorithms, further enhancing the real-time engineering performance of dynamic inversion.

Author Contributions: Conceptualization, H.G., Y.X. and Q.D.; Methodology, Q.D. and D.Y.; Software, Y.X.; Investigation, D.Y.; Resources, P.Z., S.T., Q.D. and D.Y.; Data curation, H.G. and S.T.; Writing—original draft, H.G. and Y.X.; Writing—review and editing, H.G. and Y.X.; Supervision, P.Z. All authors have read and agreed to the published version of the manuscript.

Funding: This research received no external funding.

Data Availability Statement: The original contributions presented in this study are included in the article. Further inquiries can be directed to the corresponding authors.

Conflicts of Interest: Author Peng Zhao was employed by Roc Oil (Chengdu) Limited. Author Shuang Tang was employed by CNPC (Beijing) Digital Intelligence Research Institute. The remaining authors declare that the research was conducted in the absence of any commercial or financial relationships that could be construed as a potential conflict of interest.

References

1. Akers, T.J. Improving Hole Quality and Casing-Running Performance in Riserless Top Holes: Deepwater Angola. *SPE Drill. Complet.* **2009**, *24*, 484–497. [CrossRef]
2. Chen, Y.F.; Zhang, H.; Wu, W.X.; Li, J.; Ouyang, Y.; Lu, Z.Y.; Ma, D.X.; Wu, Y.C.; Liu, J.B.; Liu, K.R.; et al. Simulation Study on Cuttings Transport of the Backreaming Operation for Long Horizontal Section Wells. *Pet. Sci.* **2024**, *21*, 1149–1170. [CrossRef]
3. Jamil, N.; Khan, M.R.; Shah, S.H.A.; Zubair; Al Maktoumi, A.S. Enhancing Drilling Efficiency Through Automated Data Management and Artificial Intelligence for Real-Time Monitoring Services. In Proceedings of the SPE EOR Conference at Oil and Gas West Asia, Dubai, United Arab Emirates, 12–14 May 2025; SPE: Richardson, TX, USA, 2025; p. D011S012R003.
4. Khazali-Rosli, K.A.; Murad, M.S.; Mokhti, M.R.; Jamal, J.; Zurhan, M.S.; Mat Noh, N.; Kereshanan, M.; Rashid, K.A.A.; Ting, S.Z.; Herrera, C.; et al. Preserving Business Resilience—AI Driven Drilling Automation as the Engine of Change for Sustainable Performance. In Proceedings of the SPE Asia Pacific Oil and Gas Conference and Exhibition, Bangkok, Thailand, 10–12 October 2023; SPE: Richardson, TX, USA, 2023; p. D012S002R013.
5. Kim, S.; Kim, T.W.; Jo, S. Artificial Intelligence in Geoenergy: Bridging Petroleum Engineering and Future-Oriented Applications. *J. Pet. Explor. Prod. Technol.* **2025**, *15*, 35. [CrossRef]
6. Li, G.S.; Shi, X.Z.; Tang, S.C. Intelligent Drilling Technology Research Status and Development Trends. *Pet. Drill. Tech.* **2020**, *48*, 1–8.
7. Ashena, R.; Rabiei, M.; Rasouli, V.; Mohammadi, A.H.; Mishani, S. Drilling Parameters Optimization Using an Innovative Artificial Intelligence Model. *J. Energy Resour. Technol.* **2021**, *143*, 052110. [CrossRef]
8. Elkatatny, S. Real-Time Prediction of Rate of Penetration While Drilling Complex Lithologies Using Artificial Intelligence Techniques. *Ain Shams Eng. J.* **2021**, *12*, 917–926. [CrossRef]
9. Haghgouei, H.; Nermoen, A.; Lavrov, A. Numerical study of material contrast effect on damage and instability in wellbores under repeated drill string impacts. *J. Rock Mech. Geotech. Eng.* 2025, *in press*. [CrossRef]
10. Song, Y.W.; Kim, I.; Lee, S.H.; Chung, C.K. Development of a Borehole Pressure Shear Test Apparatus for Evaluating the In-situ Geotechnical Properties of Intermediate Geomaterial. *KSCE J. Civ. Eng.* 2025, *in press*. [CrossRef]
11. Wu, X.; Bai, W.; Xie, Y.; Sun, X.; Deng, C.; Cui, H. A Hybrid Algorithm of Particle Swarm Optimization, Metropolis Criterion and RTS Smoother for Path Planning of UAVs. *Appl. Soft Comput.* **2018**, *73*, 735–747. [CrossRef]
12. Oden, J.T.; Martins, J.A.C. Models and Computational Methods for Dynamic Friction Phenomena. *Comput. Methods Appl. Mech. Eng.* **1985**, *52*, 527–634. [CrossRef]
13. James, G.; Witten, D.; Hastie, T.; Tibshirani, R.; Taylor, J. Unsupervised Learning. In *An Introduction to Statistical Learning: With Applications in Python*, 1st ed.; James, G., Witten, D., Hastie, T., Tibshirani, R., Eds.; Springer International Publishing: Cham, Switzerland, 2023; pp. 503–556.
14. Murtagh, F.; Contreras, P. Algorithms for Hierarchical Clustering: An Overview, II. *Wiley Interdiscip. Rev. Data Min. Knowl. Discov.* **2017**, *7*, e1219. [CrossRef]

15. Likas, A.; Vlassis, N.; Verbeek, J.J. The Global k-Means Clustering Algorithm. *Pattern Recognit.* **2003**, *36*, 451–461. [CrossRef]
16. Reddy, C.K.; Vinzamuri, B. A Survey of Partitional and Hierarchical Clustering Algorithms. In *Data Clustering*; Chapman and Hall/CRC: Boca Raton, FL, USA, 2018; pp. 87–110.
17. Zhao, Y.; Karypis, G.; Fayyad, U. Hierarchical Clustering Algorithms for Document Datasets. *Data Min. Knowl. Discov.* **2005**, *10*, 141–168. [CrossRef]
18. Delahaye, D.; Chaimatanan, S.; Mongeau, M. Simulated Annealing: From Basics to Applications. In *Handbook of Metaheuristics*; Springer International Publishing: Cham, Switzerland, 2018; pp. 1–35.
19. Lakkimsetty, N.R.; Al Araimi, H.R.A.; Kavitha, G. Modelling and Optimization of Well Hole Cleaning Using Artificial Intelligence Techniques. *Discov. Appl. Sci.* **2025**, *7*, 124. [CrossRef]
20. Tariq, Z.; Mahmoud, M.; Abdulraheem, A. Real-time Prognosis of Flowing Bottom-Hole Pressure in a Vertical Well for a Multiphase Flow Using Computational Intelligence Techniques. *J. Pet. Explor. Prod. Technol.* **2020**, *10*, 1411–1428. [CrossRef]
21. Feng, Q.; Wang, H.-J.; Zhan, H.-Y.; Ding, K.-Y.; Wu, J. Selection and Optimization of Floating Casing Technology in Field Application. In *Proceedings of the International Field Exploration and Development Conference 2023*; Lin, J., Ed.; Springer Series in Geomechanics and Geoengineering (SSGG); Springer Nature Singapore: Singapore, 2023; Volume 6, pp. 828–835.
22. Zhang, X.; Chen, Z.; Chen, X.; Wang, X.; Yuan, W.; Yang, Q. A Dual-Parameter Optimization Method of Floating Casing Technology. In Proceedings of the ARMA US Rock Mechanics/Geomechanics Symposium, Online, 18–25 June 2021; ARMA: Arlington, VA, USA, 2021; p. ARMA-2021-1683.
23. Zhang, J.; Li, J.; Li, Z.; Hu, P.; Lian, W.; Yang, H.; Han, J. Open-hole Extension Limit of Offshore Extended-Reach Well Considering Formation Collapse. *J. Pet. Explor. Prod. Technol.* **2024**, *14*, 2473–2489. [CrossRef]
24. Wang, G.; Lv, Z.; Zhong, L.; Li, Z.; Fu, Q.; Li, Y.; He, Y.; Zhang, Z. Double-layer Pipe Dual-gradient Drilling Wellbore Pressure Calculation Model and Parameters Optimization. *Geoenergy Sci. Eng.* **2023**, *230*, 212249. [CrossRef]

Disclaimer/Publisher's Note: The statements, opinions and data contained in all publications are solely those of the individual author(s) and contributor(s) and not of MDPI and/or the editor(s). MDPI and/or the editor(s) disclaim responsibility for any injury to people or property resulting from any ideas, methods, instructions or products referred to in the content.